ELSEVIER

Journal of Chromatography B, 664 (1995) 233–240

JOURNAL OF CHROMATOGRAPHY B: BIOMEDICAL APPLICATIONS

Short communication

Bioseparations with permeable particles

A.E. Rodrigues*, J.M. Loureiro, C. Chenou, M. Rendueles de la Vega

Laboratory of Separation and Reaction Engineering, Faculty of Engineering, University of Porto, 4099 Porto Codex, Portugal

Abstract

Permeable large-pore particles have many applications, in particular in perfusion chromatography for bioseparations. The objective of this paper is to elucidate the mass transport mechanisms in two commercial adsorbents–POROS Q/M and Q Hyper D–and to answer the question if intraparticle convection is present as a mass transfer mechanism. The paper contains three sections. In the first part, mass transfer inside porous particles is discussed. The mass transfer mechanism which allows improved performance of perfusion chromatography is intraparticle convection. The combined effect of intraparticle convection and diffusion is an "augmented" effective diffusivity. This is the key concept to explain the peak sharpening and modified Van Deemter plots found with large-pore particles. In the second part, column efficiencies in terms of HETP as a function of bed superficial velocity are experimentally measured for a non-retained protein (bovine serum albumine, BSA) in two adsorbents: POROS Q/M (PerSeptive Biosystems) and Q Hyper D (BioSepra). In the third section breakthrough curves for both materials are measured for a test protein (BSA) from which useful capacities and productivities as a function of flow-rate are calculated. Experimental results indicate that intraparticle convection plays indeed an important role in both adsorbents.

1. Introduction

Permeable packings are used in process chromatography, e.g. in perfusion chromatography [1,2]. Such adsorbents provide a way to reduce intraparticle mass transfer resistances by increasing the particle permeability B_p as an alternative to pellicular packings or reduction of particle size. In contrast to conventional supports, mass transfer inside permeable particles occurs by convection and diffusion; therefore, the mass transfer flux, N_i, is the sum of the diffusive and convective fluxes, i.e.

$$N_i = v_o c_i - D_e \frac{dc_i}{dz} \quad (1)$$

where v_o is the intraparticle convective velocity, D_e is the effective diffusivity, c_i is the species concentration and z is the space coordinate for the particle. The relative importance of convective and diffusive fluxes is assessed by the intraparticle Peclet number λ defined as:

$$\lambda = \frac{v_o l}{D_e} \quad (2)$$

where l is the half-thickness of the slab particle.

The intraparticle convective velocity v_o can be estimated by equating the pressure drop across

* Corresponding author.

0378-4347/95/$09.50
SSDI 0378-4347(94)00361-0

the particle $\Delta p/(2l)$ and the pressure drop across the bed $\Delta P/L$ given by Darcy's law [3,4]. This seems to be valid in HPLC applications, so

$$v_o = \frac{B_p}{B_b} u_o \tag{3}$$

where B_p and B_b are the particle and bed permeabilities, respectively and u_o is the bed superficial velocity.

The combined effect of intraparticle convection and diffusion results in an "augmented" diffusivity $\tilde{D}_e$ which can be used in simple diffusion models for process design. The concept of "augmented" diffusivity is the key concept to understand the improved performance of perfusion chromatography and was quantified as early as 1982 by Rodrigues et al. [4]:

$$\tilde{D}_e = \frac{D_e}{f(\lambda)} \tag{4}$$

The enhancement factor is $1/f(\lambda)$ where

$$f(\lambda) = \frac{3}{\lambda}\left(\frac{1}{\tanh \lambda} - \frac{1}{\lambda}\right) \tag{5}$$

At low flow-rates $\lambda \rightarrow 0$ and $\tilde{D}_e = D_e$; therefore, permeable particles behave as conventional packings. At high flow-rates $f(\lambda) \approx (1/\lambda)$ and $\tilde{D}_e = (v_o l)/3$, i.e. in the convection-controlled limit the augmented diffusivity $\tilde{D}_e$ depends only on the particle permeability and fluid properties.

The consequences of the "augmented" diffusivity $\tilde{D}_e$ on peak sharpening, peak resolution and HETP vs. u_o plots have been discussed in detail elsewhere [5–7]. Consideration of adsorption–desorption kinetics [8] and bidisperse structures [9] have also been made. In short, because of the augmented diffusivity peaks are sharper than in columns packed with conventional packings and column responses are driven by intraparticle convection from diffusion-controlled to equilibrium limits. The HETP vs. u_o plot shows interesting features: as u_o increases, HETP departures from the linear diffusion-controlled plot and goes to a plateau in the convection-controlled region. This means that HETP is lower than in conventional packings, i.e. efficiency is better with permeable particles and speed of separation can be improved without loosing efficiency.

The objective of this paper is to elucidate the mass transfer mechanisms responsible for the improved performance observed in two commercial adsorbents [1,10]–POROS Q/M (PerSeptive Biosystems, Cambridge, MA, USA) and Q Hyper D (BioSepra, Villeneuve la Garenne, France). Two kinds of experiments were performed: pulse injections of proteins under non-retaining conditions and breakthrough experiments under retaining conditions. The first series enables the determination of the column efficiencies in terms of HETP as a function of bed superficial velocity, while from the second useful capacities and productivities as a function of flow-rate are calculated.

2. Mass transfer mechanisms inside chromatographic packings

In order to elucidate mass transfer mechanisms inside chromatographic adsorbents we looked at column responses to pulse injection of test proteins under non-retaining conditions, using two different columns (POROS Q/M and Q Hyper D) with characteristics shown in Table 1.

The chromatographic experiments were carried out on a Gilson 715 HPLC system equipped with a Model 360 pump, an injection valve and a UV detector (Model 17); the system is computer controlled, and automatic data acquisition is incorporated.

Three test proteins (ovalbumin, myoglobin and BSA) from Sigma were used in the experiments; the solvent was 50 m*M* Tris-HCl (pH 8.6)–0.5 *M* NaCl and a pulse concentration of 0.3 mg/ml of protein was injected; the experiments were run at flow-rates up to 10 ml/min.

Chromatographic peaks for myoglobin obtained at various flow-rates on POROS Q/M are shown in Fig. 1, as an example. The figure shows that as flow-rate increases, peaks become sharper as a result of intraparticle convection.

The HETP as a function of bed superficial velocity has been calculated for both columns

Table 1
Characteristics of the columns used in experiments

Parameter	POROS Q/M	Q Hyper D
Bed length (cm)	10	10
Bed internal diameter (mm)	4.6	5
Particle diameter (μm)	20	35
Bed porosity	0.34	0.37
Particle porosity	0.5	–
Operating flow-rate (ml/min)	3–15	1–10

with $\mathrm{HETP} = \sigma^2 L/\mu_1^2$ (where σ^2 is the peak variance, μ_1 is the first moment of the peak or mean retention time and L is the column length). Experimental results of reduced HETP (HETP/d_p) as a function of the superficial velocity u_o for BSA are shown in Fig. 2a,b for POROS Q/M and Q Hyper D, respectively.

The shape of the HETP vs. u_o plot for POROS Q/M clearly follows Rodrigues' equation

$$\mathrm{HETP} = A + \frac{B}{u_o} + Cf(\lambda)u_o \approx A + Cf(\lambda)u_o \qquad (6)$$

The behavior of the Q Hyper D adsorbent displays, apparently, a constant HETP. Experiments at low flow-rates show, however, a rapid increase and then evolution towards a plateau. The initial slope of this plot is related with intraparticle diffusivity and the plateau with

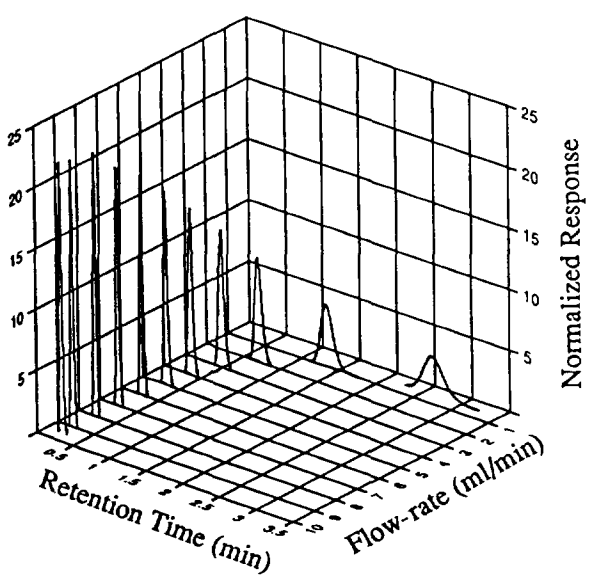

Fig. 1. Chromatographic peaks for myoglobin at various flow-rates in a POROS Q/M column.

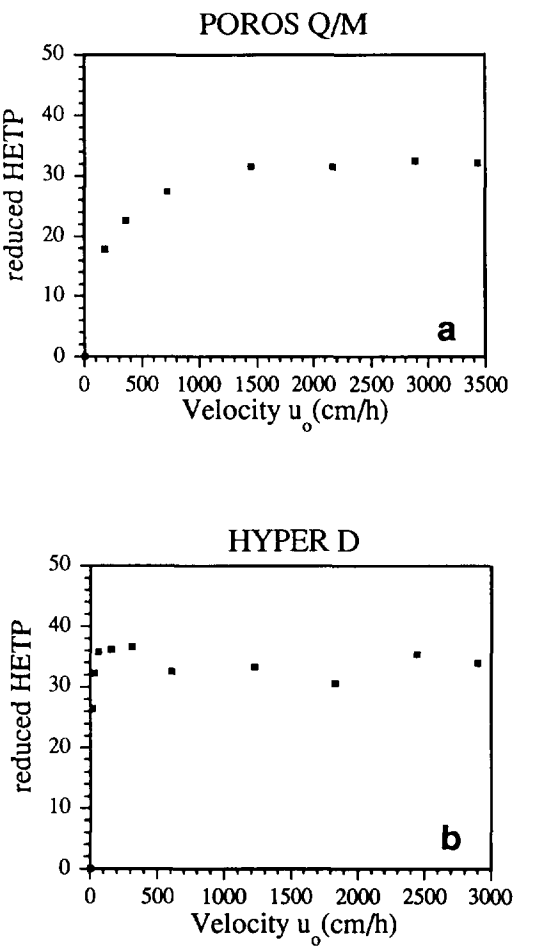

Fig. 2. Experimental reduced HETP as a function of superficial velocity for: (a) a POROS Q/M column; (b) a Q Hyper D column.

particle permeability. It seems that at small velocities low gel-diffusion dominates but as u_0 increases the slope changes and becomes dominated by pore diffusivity to finally become convection-controlled as indicated by the plateau. Estimates of particle permeability can be made if particle porosity is known.

From the measurement of column pressure drop as a function of flow-rate, bed permeabilities can be calculated. Fig. 3a,b show ΔP as a function of u_0 for POROS Q/M and Q Hyper D, respectively. For the POROS Q/M column, the bed permeability is 2.42×10^{-9} cm^2, whilst for the Q Hyper D column $B_b = 1.02 \times 10^{-8}$ cm^2.

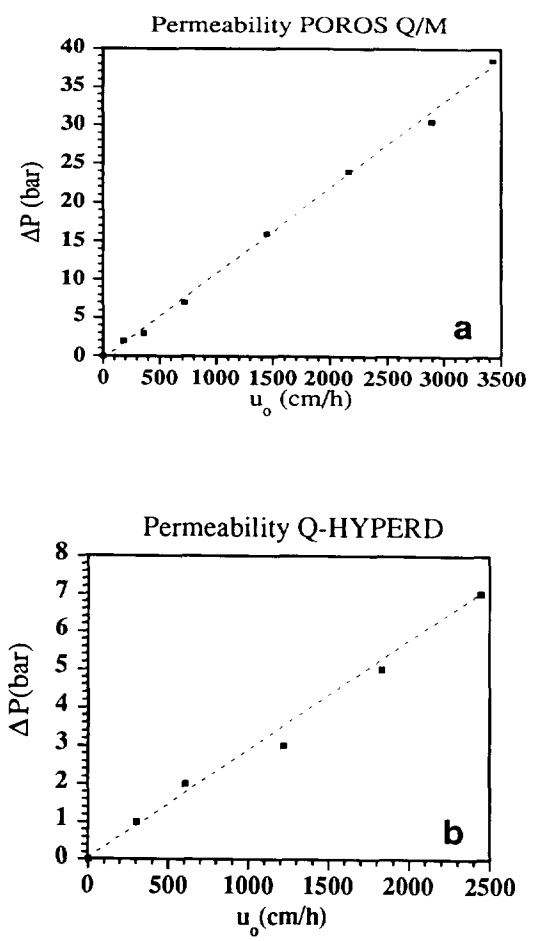

Fig. 3. Bed pressure drop as a function of superficial velocity in: (a) a POROS Q/M column; (b) a Q Hyper D column.

3. Breakthrough curves for BSA under retained conditions

Experiments were carried out with both columns under the following operating conditions: the solvent was Tris-HCl 20 m*M*, pH 8.6, the test protein is BSA (Sigma) at concentrations from 0.1 to 3 mg/ml and flow-rates up to 10 ml/min were used.

Breakthrough and desorption curves for POROS Q/M and Q Hyper D at various flow-rates are shown in Figs. 4 and 5, respectively. Elution was carried out using 20 m*M* Tris-HCl (pH 8.5)–0.5 *M* NaCl. Breakthrough curves for POROS Q/M are very sharp as a result of intraparticle convection. Normalized plots in terms of c/c_0 vs. Uc_0t (amount of protein fed to the bed) during adsorption and in terms of c/c_0 vs. Ut during desorption, shown in Figs. 6 and 7 for POROS Q/M and Q Hyper D, respectively, indicate that in this flow-rate range all breakthrough curves merge together; this seems again to be a consequence of intraparticle convection. Note that the coordinate Uc_0t used in the adsorption runs in Figs. 6 and 7 is equivalent to the more commonly used coordinate t/t_{st}, where

$$t_{st} = \frac{\epsilon V c_o + (1-\epsilon) V q_o}{U c_o}$$

is the stoichiometric time calculated from an overall material balance. During the desorption runs the UV detector saturated; this is why the curves shown exhibit a plateau. Plots of useful capacity (at the breakthrough point) and productivity, calculated by dynamic capacity/(breakthrough time × bed volume), as a function of flow-rate are shown in Fig. 8a,b for POROS Q/M and Q Hyper D, respectively. The useful capacity is almost constant in this flow-rate range and productivity increases almost linearly with flow-rate. The productivity results are similar for both adsorbents. This only means that one can process the same amount of protein in one day with both adsorbents; however, with POROS Q/M more adsorption/desorption cycles are required in one day. Also, since the capacity is higher for Q Hyper D, we will recover the

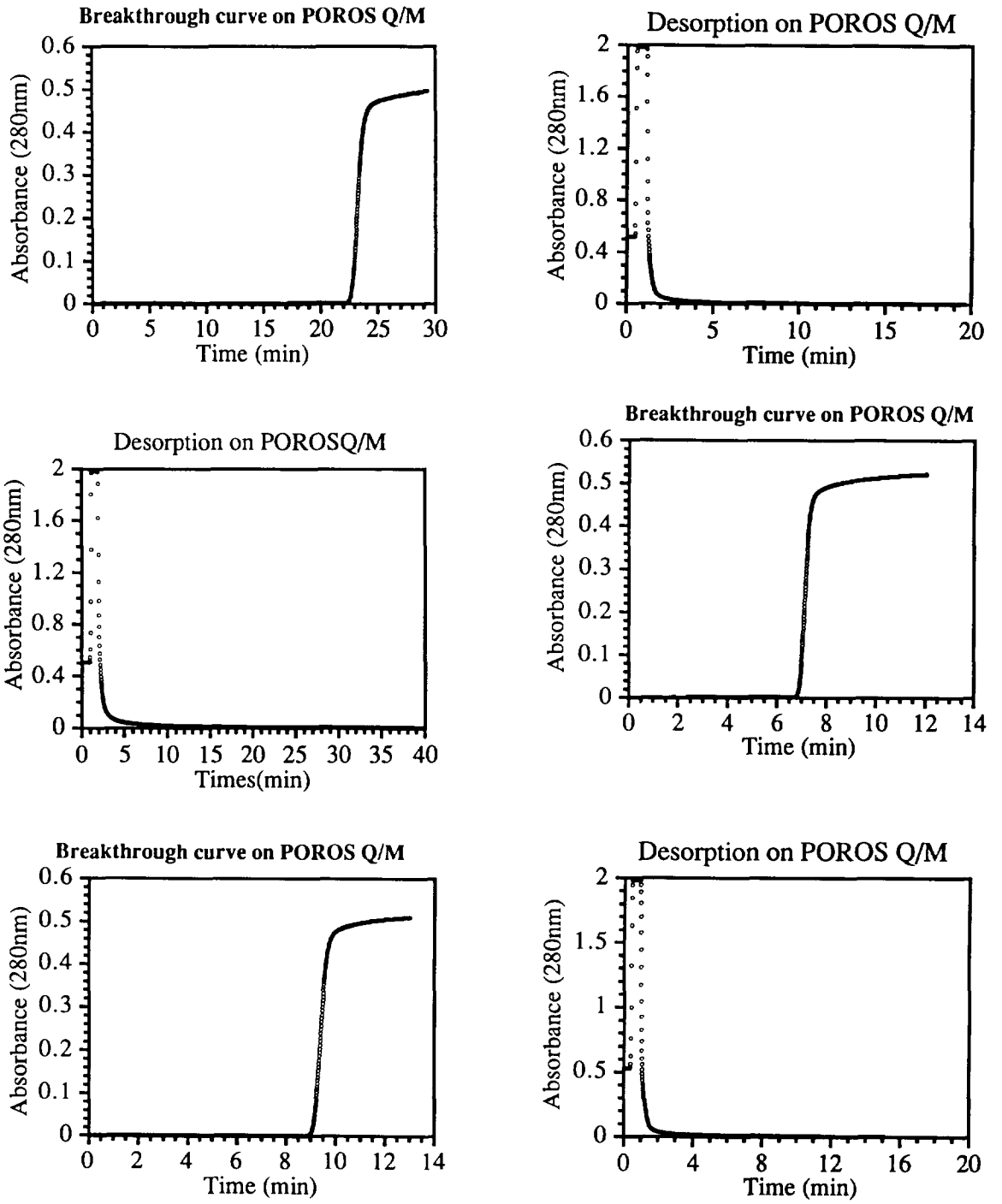

Fig. 4. Breakthrough and elution curves for BSA in a POROS Q/M column at various flow-rates ($U = 2$, 5 and 7 ml/min). The BSA feed concentration used in all breakthrough runs was 1 mg/ml; the observed pressure drop along the column was around 10, 26 and 35 bar for the flow-rates 2, 5 and 7 ml/min, respectively.

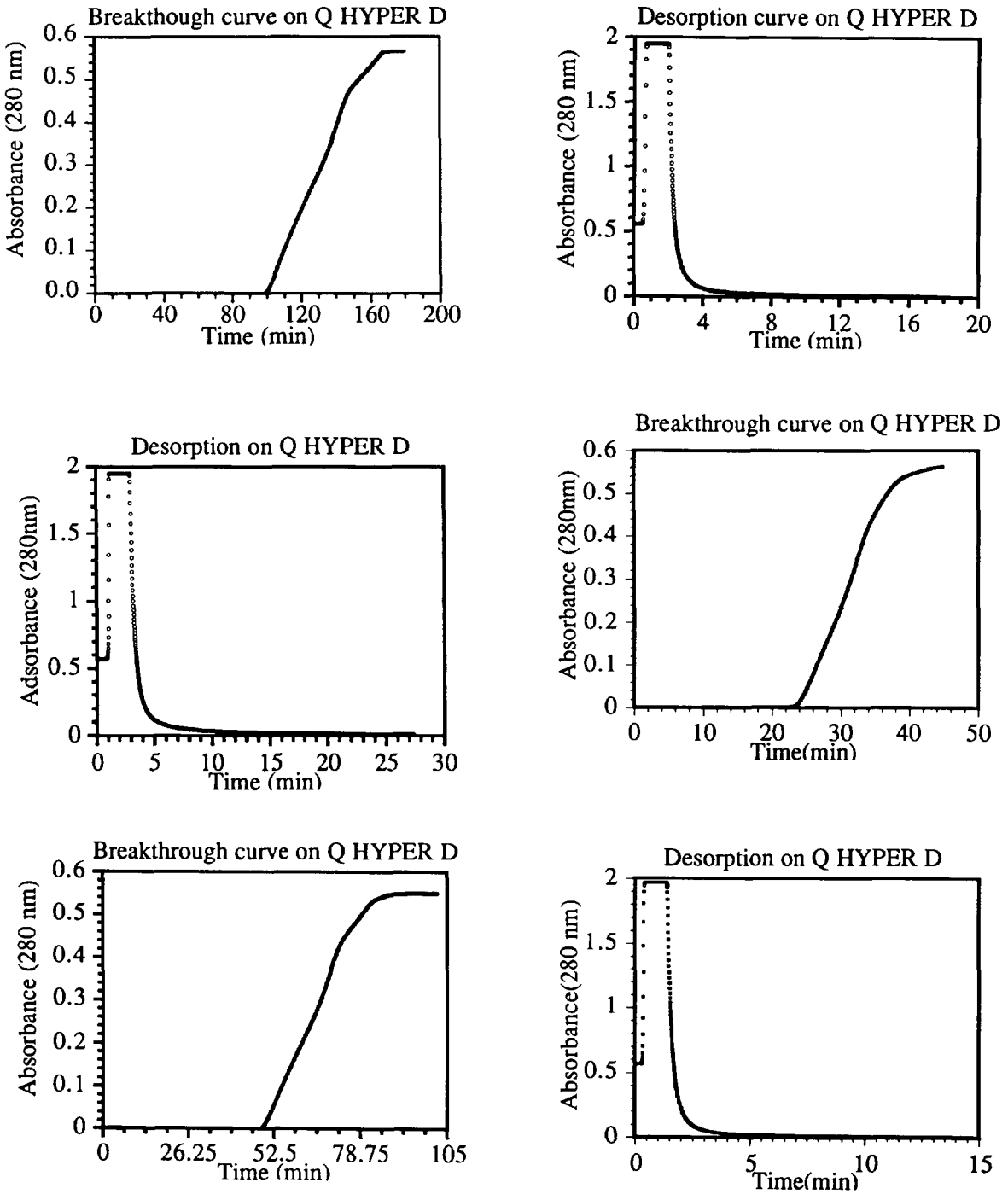

Fig. 5. Breakthrough and elution curves for BSA in a Q Hyper D column at various flow-rates ($U = 2$, 4 and 8 ml/min). The BSA feed concentration used in all breakthrough runs was 1 mg/ml; the observed pressure drop along the column was around 3, 4 and 8 bar for the flow-rates 2, 4 and 8 ml/min, respectively.

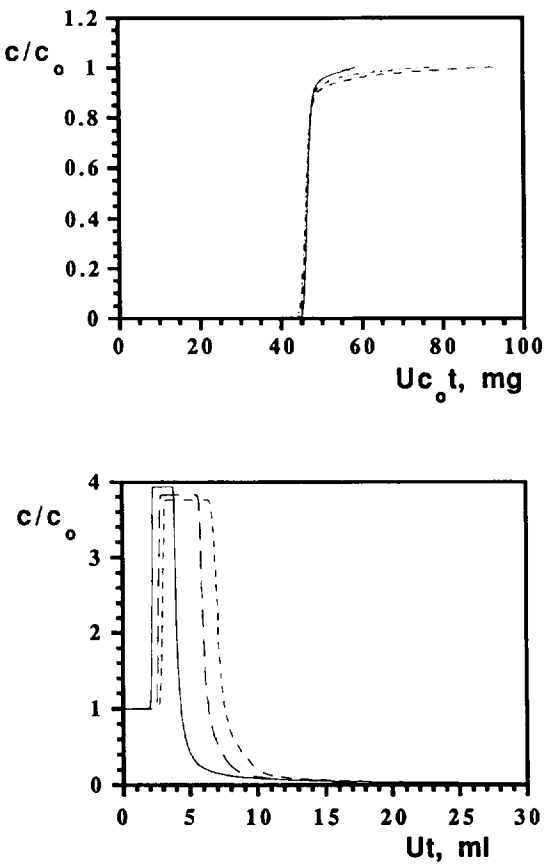

Fig. 6. Normalized breakthrough and elution curves for BSA in a POROS Q/M column at various flow-rates: (—) $U = 2$ ml/min; (- - -) $U = 5$ ml/min; (- · · ·) $U = 7$ ml/min.

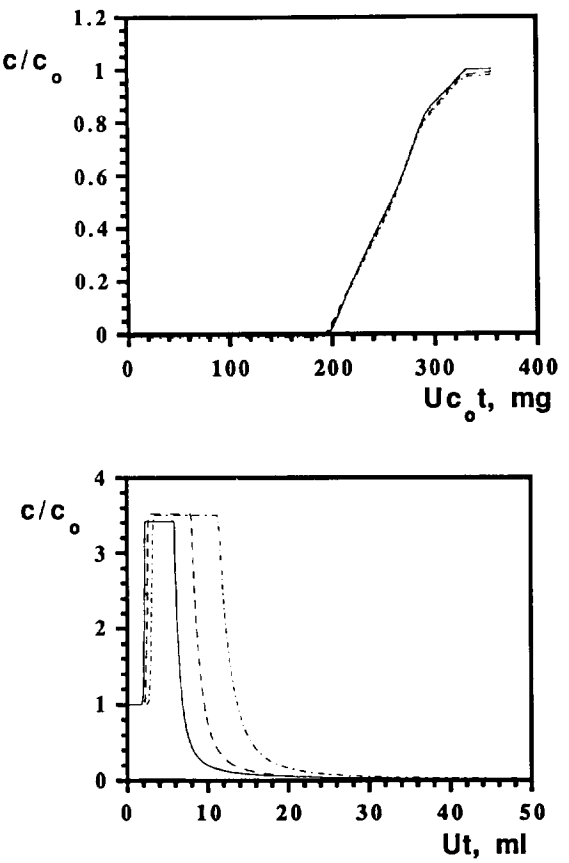

Fig. 7. Normalized breakthrough and elution curves for BSA in a Q Hyper D column at various flow-rates: (—) $U = 2$ ml/min; (- - -) $U = 4$ ml/min; (- · · ·) $U = 8$ ml/min.

protein at higher concentration in the desorption step.

4. Conclusions

Two columns packed with different materials currently used in protein separations (POROS Q/M and Q Hyper D) are compared in this work under non-retaining conditions (elution chromatography) and retaining conditions (frontal chromatography followed by regeneration).

The HETP of the POROS Q/M column clearly follows Rodrigues' equation, going to a plateau in the convection-dominated region (high superficial velocity). For the Q Hyper D column, a rapid increase of HETP is detected at very low flow-rates and then a plateau develops, as well. It seems that mass transfer control changes from gel to pore diffusion and then to convection in this material. Bed permeabilities were calculated for both columns.

The breakthrough curves for the POROS Q/M column are very sharp as a consequence of intraparticle convection. Although the Q Hyper D curves are less sharp, the normalized responses c/c_0 vs. Uc_0t (amount of protein fed to the bed) for each packing merge together; this seems again to be a consequence of intraparticle convection. For both columns the useful capacity

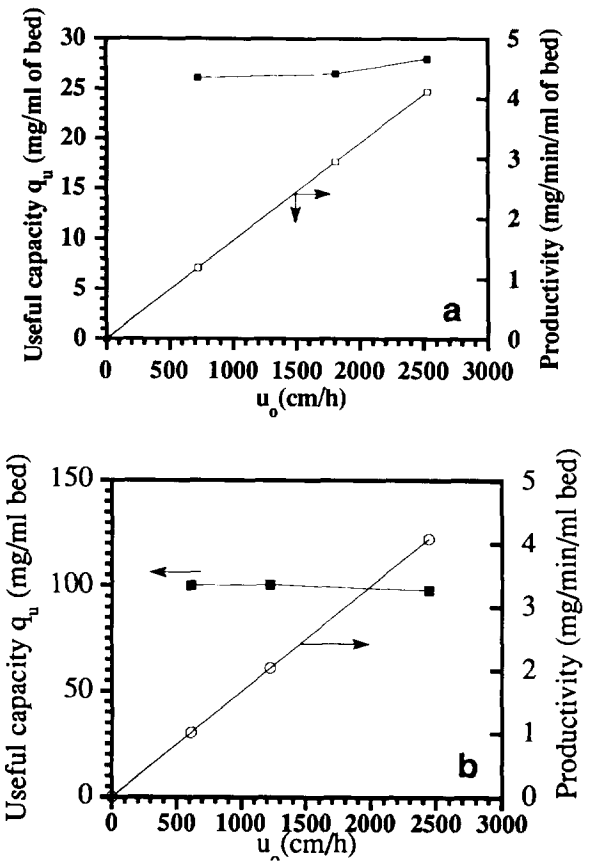

Fig. 8. Useful capacity and productivity as functions of the superficial velocity for: (a) a POROS Q/M column; (b) a Q Hyper D column.

is almost constant in the range of flow-rates studied, while the productivity increases linearly with flow-rate.

Symbols

A	Constant (Rodrigues' equation)
B	constant (Rodrigues' equation)
B_b	Bed permeability
B_p	Particle permeability
C	Constant (Rodrigues' equation)
c	Outlet concentration (breakthrough experiments)
c_o	Feed concentration (breakthrough experiments)
c_i	Concentration of species i
d_p	Particle diameter
D_e	Intraparticle effective diffusivity
$\tilde{D}_e$	"Augmented" (by intraparticle convection) intraparticle effective diffusivity
$HETP$	Height equivalent to a theoretical plate
L	Bed length
l	Half-thickness of the slab particle
N_i	Intraparticle mass transfer flux of species i
Δp	Pressure drop across the slab particle
ΔP	Pressure drop across the bed
q_o	Adsorbed phase concentration in equilibrium with the feed concentration c_o
t	Time
t_{st}	Stoichiometric time
U	Flow-rate
u_o	Bed superficial velocity
V	Bed volume
v_o	Intraparticle convective velocity
z	Space coordinate for the slab particle

Greek symbols

λ	Intraparticle Peclet number
μ_1	First moment of the peak (mean retention time)
σ^2	Variance of the peak

References

[1] N. Afeyan, F. Regnier and R. Dean, Jr., U.S. Patent no. 5,019,270, May 28, 1991.
[2] N. Afeyan, F. Regnier and R. Dean, Jr., U.S. Patent no. 5,228,989, July 20, 1993.
[3] H. Kommiyama and H. Inoue, *J. Chem. Eng. Jpn.*, 7 (1974) 281.
[4] A.E. Rodrigues, B. Ahn and A. Zoulalian, *Am. Inst. Chem. Eng. J.*, 28 (1982) 541.
[5] A.E. Rodrigues, Z.P. Lu and J.M. Loureiro, *Chem. Eng. Sci.*, 46 (1991) 2765.
[6] A.E. Rodrigues, J.C. Lopes, Z.P. Lu, J.M. Loureiro and M.M. Dias, *J. Chromatogr.*, 590 (1992) 93.
[7] A.E. Rodrigues, *LC-GC*, 6 (1993) 20.
[8] A.E. Rodrigues, A.M.D. Ramos, J.M. Loureiro, M. Diaz and Z.P. Lu, *Chem. Eng. Sci.*, 47 (1992) 4405.
[9] A.E. Rodrigues, Z.P. Lu and J.M. Loureiro, *J. Chromatogr. A*, 653 (1993) 189.
[10] E. Boschetti, *J. Chromatogr. A*, 658 (1994) 207.